LBL-12729

CONF-810750--9

Lawrence Berkeley Laboratory
UNIVERSITY OF CALIFORNIA

Materials & Molecular
Research Division

Presented at the Second National Conference on Synchrotron Radiation Instrumentation, Cornell University, Ithaca, NY, July 15-17, 1981; and to be published in Nuclear Instruments and Methods

PERFORMANCE AND APPLICATION OF A DOUBLE-CRYSTAL MONOCHROMATOR IN THE ENERGY REGION 800 ≤ hν ≤ 4500 eV

Z. Hussain, E. Umbach, D.A. Shirley, J. Stöhr, and J. Feldhaus

July 1981

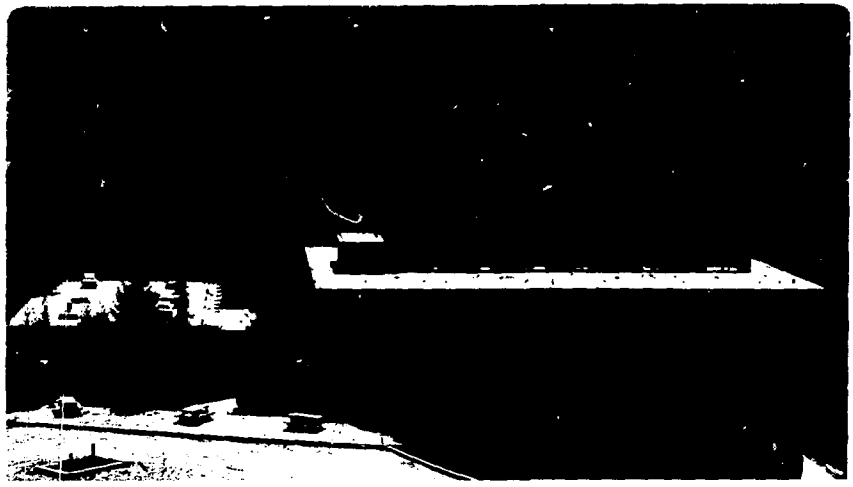

Prepared for the U.S. Department of Energy under Contract W-7405-ENG-48

PERFORMANCE AND APPLICATION OF A DOUBLE-CRYSTAL MONOCHROMATOR IN THE ENERGY REGION 800 ≤ hν ≤ 4500 eV

Z. Hussain,* E. Umbach,† and D. A. Shirley

Materials and Molecular Research Division
Lawrence Berkeley Laboratory
and
Department of Chemistry
University of California
Berkeley, California 94720

J. Stöhr‡ and J. Feldhaus§

Stanford Synchrotron Radiation Laboratory
Stanford University
Stanford, California 94305

*Present Address: University of Petroleum and Minerals
Dhahran, Saudi Arabia.

†Permanent Address: Physik-Department, Technische Universität München
West Germany.

‡Present Address: EXXON Research and Engineering Company, P.O. Box 45,
Linden, N.J. 07036.

§Permanent Address: Institut für Atom- und Fest körperphysik,
Freie Universität, Berlin, D-1000 Berlin 33,
West Germany.

ABSTRACT

The performance and application of an ultra-high-vacuum compatible constant-deviation double-crystal monochromator (JUMBO) in operation at SSRL is demonstrated. The monochromator can be operated with any of four pairs of crystals interchangeable *in situ*. An electronic-maximum-search feedback loop optimizes the intensity of the spatially fixed outgoing beam as the photon energy is scanned. The monochromatic beam is focussed (~1.5 mm x 5 mm) onto the sample by a toroidal mirror. Monochromator crystals of beryl(10$\bar{1}$0), InSb(111) and Ge(111) have been tested in the energy regions 800-1540 eV, 1690-4000 eV and 1930-4500 eV, respectively. The performance of these crystals with regard to the resolution, the intensity, the level of scattered light, and the contribution of higher orders have been determined. Various effects arising from a radiation-induced temperature gradient in the monochromator crystals are discussed. Novel studies of bulk and surface properties of materials by angle-resolved photoemission, x-ray induced Auger spectroscopy, photon-stimulated ion desorption, bulk and surface extended x-ray absorption fine structure (EXAFS and SEXAFS) measurements in this previously inaccessible energy region of the electromagnetic spectrum are also discussed.

I. INTRODUCTION

A serious constraint on experimental spectroscopy is the limited energy range over which suitable light sources are available. Before the utilization of high-energy electron accelerators, intense tunable light sources were available only for energies up to the ultraviolet range ($h\nu \lesssim 10$ eV). During the 1970's synchrotron radiation, with appropriate monochromators, has extended this range considerably. The unique properties of synchrotron radiation have resulted in new experimental developments in various fields of science which have lead to a rapid growth of synchrotron radiation facilities in many countries [1]. The widest energy range is, at present, covered at the Stanford Synchrotron Radiation Laboratory (SSRL).

The method utilized for monochromatizing synchrotron radiation depends on the energy range of interest. Normal incidence monochromator are employed in the vacuum ultraviolet (VUV) region from ~5 to 40 eV (2000-300 Å) while grazing incidence monochromators are employed in the energy region from ~30 to 800 eV (400-20 Å) [2,3]. In the hard x-ray energy regime, above 3 keV ($\lesssim$4 Å), crystal monochromators are operated under an atmospheric pressure of helium gas, which must be separated from the storage ring vacuum by beryllium windows, thereby restricting the lower energy limit of transmitted radiation to $\lesssim$3 keV. The remaining spectral gap in the soft x-ray region (800-3000 eV) could in principle be covered by either grating or crystal monochromators. However, the application of grating monochromators in this energy region is limited by their relatively poor resolution and their low monochromatic-to-scattered light contrast ratio at higher energies.

With the explicit goal of closing the gap in available photon energies while at the same time maintaining high resolution, a double crystal vacuum monochromator was designed and installed at SSRL [5]. The design of this instrument was specifically optimized for use with the SPEAR storage ring,

and it combines the technologies previously used in the VUV and hard x-ray spectral regions. The monochromator first produced monochromatic light in March 1980. It is now in continuous operation at SSRL. In this paper, we will discuss the performance and application of this ultrahigh-vacuum (UHV) compatible constant deviation double-crystal monochromator (JUMBO) which presently covers the spectral range from 800 to 4500 eV [6].

The structure of the paper is as follows. After summarizing the important design features in Section II, we describe the electronic-maximum-search feedback loop in Section III. In Section IV the performance of each monochromator crystal material is discussed with regard to its spectral resolution, transmission function, photon intensity, the level of scattered light, and the contribution of higher orders. Some absorption spectra are given for illustration purposes. Section V deals with various radiation-induced temperature effects. The application of this spectral region to various scientific problems is illustrated by selected examples in Section VI. Our conclusions and suggestions for future developments are presented in Section VII.

II DESIGN FEATURES

The optical and mechanical design of the double-crystal monochromator (JUMBO) has been described in detail by Cerino et al [5]. Here, we briefly summarize its important features.

The main objectives were to design a beam line which (1) produces monochromatic radiation in the ~500-4500 eV range with photon resolution within 0.3-2.0 eV, (2) provides a high intensity focused beam of small size ($\sim 1 \times 3$ mm^2) at the sample position, (3) yields a spatially fixed beam behind the monochromator, and (4) is UHV ($\sim 10^{-10}$ torr) compatible. These objectives reflect the anticipated use of the line for high resolution soft x-ray

photoemission, near-edge absorption fine structure, and EXAFS/SEXAFS studies along with the use of other techniques which require an UHV environment and/or a small focused light spot.

A schematic design of JUMBO is shown in Fig. 1. The synchrotron radiation traverses an entrance slit and is focused by a bent-cylindrical mirror [7] through the distant monochromator onto the sample. This platinum coated fused quartz mirror intercepts up to 10 mrad of synchrotron radiation and deflects the beam vertically by 2^{o} (grazing angle of incidence of 1^{o}). The approximately toroidally shaped mirror was designed to provide a 1 : 1 focus of the source (1 mm high x 3 mm wide) onto the sample. In practice the focused spot size is ~1.5 mm x 5 mm. A slight increase in the spot size is due mainly to imperfections introduced by bending the cylindrical mirror and probably due also to thermal expansion created by the intense flux of radiation. With a 1^{o} angle of incidence, the Pt-coated mirror is expected to eliminate radiation above ~4.3 keV but we observe intensity up to 4.5 keV, noting a gradual decrease with increasing energies as will be discussed in Section IV.3.

The effect of incorporating either of the two available entrance slits (see Fig. 1) of 1 mm and 3 mm vertical size is to provide ~30 arc sec and ~60 arc sec vertical angular opening, respectively. Because the vertical divergence of 2000 eV synchrotron radiation during dedicated running time at SSRL is ~40 arc sec, one would not expect to observe a significant improvement of resolution by collimating the beam. However, the slits allow one to control the total thermal load on the crystals which helps to minimize strain-induced broadening of the crystal rocking curves and also to avoid other temperature effects (e.g., spatial movement of the output beam) at the expense of reduced flux. This will be discussed in more detail in Section V.

The overall concept shown in Fig. 1(a) differs from the double-crystal monochromator implemented by Hastings et al [8] in that the present design has two independently rotating crystals and a crystal translation in order to maintain a fixed exit beam as shown in Fig. 1(b). The implications of utilizing two independent crystal rotations in a double-crystal monochromator will be discussed in connection with temperature effects in Section V. Furthermore, it should be stressed that JUMBO is a UHV compatible monochromator: thus no windows are used in the beam line, which maximizes the photon flux at the lower energies.

The JUMBO mechanism places all high precision goniometers outside the vacuum system and transmits motions through all metal linkages and bellows [5]. The linkages provide for a full 60^{o} rotation of the crystals corresponding to a Bragg angle range of $20^{o} \leq \Theta_{B} \leq 80^{o}$. Since no crystal covers the entire 800 to 4500 eV energy range satisfactorily, a mechanism for in situ interchangeability of crystals is incorporated which allows the user to select any four pairs of available crystals. Although the interchangeability of crystals is quite simple, limited mechanical reproducibility still necessitates 4-8 hours of realignment after each change. More details about in situ interchangeability of monochromator crystals are discussed in Section IV.1.

III MAXIMUM SEARCH FEEDBACK LOOP

The most crucial requirement for a double-crystal monochromator is the capability of keeping the Bragg planes of the two monochromator crystals parallel. The required accuracy is determined by the narrowest rocking curve of any one of the monochromator crystals. Double crystal rocking curve widths for crystals usable in the 500-5000 eV spectral range [5]are usually in excess of 50 arc sec. Thus, in scanning the monochromator the Bragg planes of the two crystals have to remain aligned with respect to

each other to better than this value. In practice the alignment and reproducibility requirements are much more stringent, because intensity fluctuations in the monochromator transmission function caused by misalignment of the Bragg planes will manifest themselves as noise in a recorded absorption spectrum. Typically the throughput intensity should not vary by more than 1% as the monochromator is scanned in energy. From the shape of the double-crystal rocking curves discussed in Section IV.2 it is then clear that the Bragg planes must remain aligned to each other to better than 5 arc sec. For JUMBO this is achieved by an analog electronic feedback loop shown in Fig. 2. The basic idea is to keep the monochromator output intensity optimized by tuning the incidence angle of one of the crystals.

The beam reflected by the focusing mirror first traverses a high transmission (~80%) metal grid. The electron yield current from this grid serves as a reference signal. The signal ($\sim 10^{-5}$ amps) is amplified by a picoammeter which provides an output voltage (V_t) proportional to the input current. A similar metal grid behind the monochromator intercepts the monochromatized radiation. Because of its lower intensity the electron yield signal from this grid is first amplified by a high current spiraltron electron multiplier (SEM). A floating battery box provides the high voltage for the SEM collector and its output current ($\sim 10^{-8}$ amps) is amplified again by a picoammeter. The resulting I_0 signal is used to normalize the signal from the sample (e.g. in an EXAFS experiment) and also serves as the primary signal (V_0) for the analog feedback loop which controls the rotation of one of the monochromator crystals. A voltage divider is used to normalize the signal V_0 to possible intensity fluctuations of the storage ring SPEAR by forming the ratio V_0/V_t. High frequency noise (~30Hz) is eliminated by a low-pass filter. The signal is then differentiated and if the derivative is found to be zero a stop pulse is provided by a comparator.

This stop pulse is sent to the CAMAC step motor controller for the goniometer which rotates the first (input) monochromator crystal.

In practice the monochromator is scanned through computer control by first moving the second (output) goniometer to the required Bragg angle (photon energy). The second crystal only receives monochromatic light and thus is much more stable in temperature than the first one. The first (input) crystal is simultaneously rotated to a calculated position which is set at a few hundred arc sec away from its ideal position where it would be in phase with the second crystal. After the second (output) crystal has reached its proper position, the first crystal is set to move. With this crystal moving closer to its ideal position the output photon intensity will follow exactly a double-crystal rocking curve. The maximum search feedback loop then stops the rotation of the first crystal at the top of the rocking curve (maximum output intensity). This scheme keeps the two crystals aligned to approximately 5-15 arc sec depending on the rocking curve width.

IV PERFORMANCE OF JUMBO

IV.1 Monochromator Crystals and Energy Range

The crystals which allow the range 550-4500 eV to be covered by JUMBO are shown in Fig. 3. Also shown are the elements with K absorption edges in this energy region. If L and M edges are also included, nearly all elements heavier than oxygen are accessible. The monochromator crystals such as beryl(10$\bar{1}$0), InSb(111) and Ge(111) have already been tested. The diffracting crystal beryl [$Be_3Al_2(SiO_3)_6$] [9] -- a naturally occurring mineral -- with 2d spacing between the (10$\bar{1}$0) planes of 15.92 Å provides highly monochromatic light of good intensity from 800 eV to 2000 eV. The intensity above ~1550 eV (Al K edge) has structure and is attenuated by the absorption of Al and Si (the Si K edge lies at 1840 eV). InSb(111) [10] with 2d = 7.4806 Å can be used from 1690 to 4000 eV. This crystal is specifically

suitable for work on the important K edge of Si. Ge(111) with 2d = 6.532 Å exhibits excellent diffraction properties, thermal stability and resolving power. The Aℓ K edge, which cannot be reached by InSb(111) or Ge(111) and is not covered by beryl satisfactorily, will be covered by α-quartz (10$\bar{1}$0) [11] with 2d = 8.512 Å corresponding to an energy region of ~1480-3700 eV. To expand the spectral range presently covered by JUMBO, we are planning to test Na β-alumina ($NaAℓ_{11}O_{17}$) [12] with 2d = 22.49 Å in the near future. This crystal will span an energy range from ~550 to 1500 eV; however, neither a high reflectivity nor a structureless transmission function can be expected in this energy range because of expected strong absorption near the K edges of O, Na and Aℓ. We also plan to test the characteristics of Mg β-alumina ($MgAℓ_{11}O_{17}$) which might be more suitable provided a good quality crystal is available.

IV.2 Rocking Curves and Energy Resolution

The inherent resolution capabilities of various crystals were assessed by measuring double-crystal rocking curves. This is easily done with JUMBO, because it operates in the so called nondispersive (1,-1) parallel mode in which two identical crystals are placed parallel to each other so that radiation is reflected first off one and then the other. For this purpose the first crystal was set at an angle corresponding to a specified photon energy and the second crystal was then rocked in Bragg angle through a plane parallel to the first crystal. The outgoing monochromatized radiation was measured by monitoring the total electron yield from a target. The results of such measurements for the beryl crystal at photon energies of 810 eV, 1000 eV, 1250 eV and 1500 eV are shown in Fig. 4. The measured double crystal rocking curve is the convolution of the incident beam angular profile and the actual rocking curves of the first and the second crystal [13]. A small vertical slit of 1 mm height was used in the above measurements,

leading to an effective angular opening of ~30 arc sec due to the combined effect of the slit and the 1 mm vertical size of the electron bunch in the storage ring. Neglecting the contribution of the angular opening of the synchrotron radiation and assuming a Gaussian shape for the rocking curve it can be shown that the actual rocking curve width of the single crystal is at least $\sqrt{2}$ lower than the measured full width at half maximum height (FWHM) (Fig. 4).

The results are summarized in Fig. 5. They clearly show that one can expect line widths between 0.35 and 0.8 eV in the energy region between 800 and 1500 eV. The 0.6 eV resolution obtained with beryl at 1100 eV should be compared with the measured value of 1.5 eV for K.A.P. [6]. The double-crystal rocking curves for InSb(111) and Ge(111) were also determined and the results are also shown in Fig. 5. InSb(111) crystals cover the energy range from 1685 to 4000 eV, including the important Si K edge. However, it is advantageous to use Ge(111) crystals above 2000 eV for experiments which require higher energy resolution.

IV.3 Transmission Functions, Intensities and Polarization

The transmission functions of JUMBO in the 800-4500 eV range using beryl ($10\bar{1}0$), InSb(111) and Ge(111), with each crystal covering a different energy region, are shown in Figs. 6-8. The transmission function for beryl indicates that the flux gradually increases from 800 eV to 1550 eV with absolutely no structure present in this range (Fig. 6). It is worthwhile to point out that the selection of a naturally occurring beryl crystal was done very carefully to avoid impurities such as Na and Mg which have K absorption edges in this energy region. The presence of Al and Si in beryl as major constituents leads to sharp structures in the transmission function above 1550 eV. This structure in the transmission function may cause problems in experiments in which the photon energy is swept. However,

photoemission experiments can still be performed satisfactorily in this region.

Fig. 7 shows the transmission function using InSb as monochromator crystals in the energy range 1800-4000 eV. The structures at the Pt M edges arise from absorption of the radiation by the platinum-coated toroidal focusing mirror. It is interesting to note that a relatively small modulation occurs due to the absorption near the In L_{III} edge (~13% absorption) at ~3730 eV and the L_{II} edge at ~3940 eV. The crystal glitches near 2030 eV, 2865 eV and 3170 eV are caused by multiple Bragg reflections from the main high symmetry diffracting plane and some low symmetry plane in the InSb monochromator crystals. It will be shown in Section IV.5 that in practice it is possible to normalize out completely the structures present in the transmission function.

The transmission function of JUMBO using Ge(111) monochromator crystals covering the energy region from 2000 to 4500 eV is shown in Fig. 8. In addition to the structures from the Pt M edges, four crystal glitches between 3400-3700 eV are present. Furthermore, it is interesting to note that no sharp mirror cutoff is observed even up to 4500 eV, in contradiction to the expected cutoff value of ~4300 eV.

The absolute photon flux from the Ge monochromator crystals was measured by inserting a beryllium window at the output of JUMBO and utilizing a gas ionization chamber. The measured photon flux from Ge(111) with SPEAR operating under dedicated conditions of ~3.0 GeV and ~50 mA is shown at the right hand side of Fig. 8. It is interesting to compare the theoretically expected flux with the measured values. If we assume a 50% mirror reflectivity and 20% Bragg reflectivity of the monochromator crystals, at least 2% of the flux emitted by SPEAR in the bandwidth of the monochromator should be expected. This value, under dedicated conditions of ~3.0 GeV and ~50 mA for a band

pass of 1 eV, corresponds to ~10^{11} photons sec^{-1} which is in excellent agreement with the measured value from the Ge(111) monochromator crystals. The 2% efficiency of JUMBO should be compared to the ~0.1% efficiency [14] of the Grasshopper [15] in the 500-1000 eV range.

The available photon fluxes from beryl and InSb, which were estimated by comparison of total electron yield signals obtained with Ge(111) at identical Bragg angles, are also shown in Figs. 6 and 7. We believe that this estimation of the flux is correct at least within ~50%.

The intrinsic high degree of linear polarization of synchrotron radiation in the plane of orbit is significantly enhanced by the double Bragg reflection geometry in the monochromator. For a vertical plane of incidence (defined by the incident ray and the crystal normal) the vertical component of the polarization is suppressed by a factor $\cos^4(2\theta_B)$ relative to the horizontal component [16]. Thus for Bragg angles around 45^o the radiation exiting from JUMBO is essentially 100% polarized. Even for the smallest (~20^o) and largest (~80^o) Bragg angles the degree of linear polarization in the horizontal plane exceeds 90%.

IV.4 Examples

In this section we illustrate some examples of near-edge and extended x-ray absorption fine structure (EXAFS) spectra obtained using these crystals in JUMBO. The first example of an EXAFS spectrum employing beryl is illustrated in Fig. 9. It shows the sodium K edge absorption fine structure in crystalline sodium chloride recorded by means of total electron yield. The resolution estimated from the leading tail of the absorption spike at threshold is better than 1.0 eV. The experimental resolution was furthermore determined from photoemission spectra of the W $4f_{7/2}$ core level, the FWHM of which was found to be 0.9 eV at a photon energy of 1100 eV.

Accounting for the finite energy resolution of the photoelectron analyzer, this value is in good accordance with the measured rocking curve widths.

Fig. 10 shows the Si K edge EXAFS spectrum obtained from a Si(111) single crystal with a (7 x 7) surface structure. This curve was obtained with the InSb monochromator crystals by measuring the total electron yield from the sample. Finally, Fig. 11 illustrates the S K edge fine and extended fine structure in NiS using the Ge(111) crystals. The FWHM of the peak near the edge is only 1.6 eV indicative of the high resolving power of the Ge(111) monochromator crystals.

IV.5 Normalization and Stray Light

The transmission function of JUMBO obtained using InSb(111) and Ge(111) monochromator crystals (Figs. 7 and 8) showed the presence of pronounced structures near the M edges of Pt. Additional sharp structures were also observed which arose from multiple Bragg scattering in the InSb(111) and Ge(111) monochromator crystals. The question arises whether it is possible to normalize out these structures in experiments which require scanning of the photon energy. As it will be shown below, it is in practice possible to normalize out completely the structures present in the transmission function.

Fig. 12 shows total yield EXAFS spectra obtained from a fused quartz (SiO_2) sample near the Si K edge using InSb crystals. Structures arising from the absorption of radiation near the Pt M edges is present in both the total yield signal (I_0) from a grid monitoring the incoming flux to the sample and in the signal from the sample (I_s). Dividing the sample signal I_s by the incoming flux I_0 totally eliminates the structures present near the Pt M edges within statistical noise of ~0.2%. As discussed previously [17], this is a strong indication that the outgoing monochromatized radiation can have only a very insignificant fraction of scattered light.

The major source of scattered light in a crystal monochromator, aside from higher orders, arises from specular reflection of radiation from the surfaces of the monochromator crystals which for low energies ($h\nu$ < 30 eV) act as mirrors. The scattered light problem in JUMBO was overcome by employing two different techniques: (1) The visible and hard ultraviolet radiation was significantly filtered by inserting one of four available graphite filters of varying thickness (0.2 - 5 μm) between the focusing mirror and the monochromator crystals. These filters cause an insignificant attenuation of radiation above 1 keV. (2) One of the monochromator crystals was cut with the surface plane slightly offset ($\sim 1^0$) from the Bragg plane, which makes the emerging scattered light propagate along a direction different from that of the monochromatized light. By employing the above two methods, it is possible to achieve monochromatized light output of better than 99% purity from JUMBO.

For Ge(111) and InSb(111) the output beam is free of higher orders due to the mirror cutoff above 5 keV and the fact that the next harmonic occurs at three times the first-order value. For beryl, higher orders are conveniently suppressed in the 800-1500 eV range by the strong absorption of Aℓ and Si present in the crystal. Photoemission spectra from metals in the energy range 900-1400 eV exhibit less than 1 count/sec above the Fermi level. Since any counts above the Fermi level can be due only to high-energy electrons ejected by stray light of higher energies, this is strong evidence for high spectral purity of the radiation.

V. THERMAL EFFECTS AND RADIATION DAMAGE

Among the important concerns associated with the use of synchrotron radiation are effects created by radiation-induced thermal loading of various optical elements. This problem becomes more severe in vacuum where no heat can be transferred by convection. In JUMBO, the total power dissipated

onto the focusing mirror can range from ~10 to 100 watts depending on beam conditions in the SPEAR storage ring and the choice of the entrance slit in front of the mirror. At a 1^{o} angle of incidence, radiation above ~4.5 keV is mostly absorbed by the mirror but the monochromator crystals are still exposed to significant power levels. However, only the first crystal is exposed to high power levels of radiation, while the second crystal sees only the monochromatized light. Thus the first crystal is most likely to be affected by radiation damage. Furthermore, the temperature difference between the crystals gives rise to a difference in lattice spacing, leading to additional problems. This Section deals with various effects arising from thermal loading of the crystals which have been observed in the JUMBO monochromator.

V.1 Thermal Effects

In the present setup of the monochromator, the second crystal is set to a calculated Bragg angle and the first crystal is continuously tuned until it is in phase with the second crystal. Fig. 13 shows the difference between the optimized angle of the first crystal and its ideal calculated Bragg angle value as the photon energy is scanned from 2000 to 3200 eV for two different entrance slits. Under perfect conditions in the monochromator, the difference should be expected to be a constant straight line. We would like to emphasize that these measurements were reproducible and were only possible after an elaborate and careful redesign of the coupling mechanism between the goniometer to the crystal-carousel assembly. The following interpretations can be made about the curves shown in Fig. 13: (1) Both curves have an oscillatory period of 1^{o} with a total amplitude of ~30 arc sec. These oscillations are related to the fact that the two Huber goniometers do not exactly track each other for 1^{o} revolutions. (2) Apart from these oscillations, there is initially at lower energies a rapid increase

in the difference function, which reaches asymptotic values at higher energies. The overall corrections required to keep the crystals in phase are 400 and 155 arc sec for curves (a) and (b), respectively. These corrections arise from different d spacings of the two monochromator crystals because of the difference in temperature. Simple model calculations with a temperature difference of 300 K for curve (a) and 150 K for curve (b) are shown as dotted lines which fit the experimental curves very well. Direct measurements of the temperature of the crystals using an infrared pyrometer indicate values which are in agreement with the theoretically calculated values.

Another extremely important effect introduced by the temperature difference is a change and non-linearity of the energy scale. This effect is shown in Fig. 14 where calculated differences between intended and actual photon energies are plotted against intended energies for various temperature differences (ΔT) of the two Ge(111) monochromator crystals. Obviously these effects cannot be neglected.

The theoretically predicted change in energy scale due to radiation-induced differential temperatures of the monochromator crystals has also been observed experimentally. Fig. 15 shows sulfur 1s photoemission spectra obtained by selecting two different sizes of entrance slits. Changing the slit size from 1 mm to 3 mm exposes the top monochromator crystal to a larger flux of incident radiation resulting in an increase of the 2d spacing of the crystal. This change results in an energy-scale shift of 1.2 eV, as shown in the figure. Furthermore, the FWHM of the photoemission peak increases from 2.25 eV to 2.75 eV, which is indicative of the decrease in resolution caused by varying the slits. With 1 mm vertical dimension of the electron bunch in the SPEAR storage ring, the divergence of the radiation through 1 mm and 3 mm slits corresponds to ~30 arc sec (1.4×10^{-4} radians) and ~60 arc sec (2.8×10^{-4} radians) respectively. Since

the natural divergence of synchrotron radiation itself is ~40 arc sec (1.8×10^{-4} rad.) at ~3 GeV, the observed increase in linewidth cannot be attributed only to the increase in slit size. We believe that the observed increase in linewidth of the photoemission peak is due mainly to an increase in lattice stress in the monochromator crystals caused by additional radiation.

These temperature effects furthermore make the alignment of the monochromator very difficult and tedious. It is particularly difficult to keep the outgoing monochromatized beam fixed in space if the power loading on the first crystal changes with time. A necessary step in further improving the performance of JUMBO definitely requires either cooling of the top crystal or perhaps controlled heating of the lower crystal to compensate for the temperature increase of the top crystal. Any procedure which makes the difference in temperature of the monochromator crystals less than $50^{o}C$ should be sufficient to avoid the aforementioned effects.

V.2 Radiation Damage

Beryl was expected to be most vulnerable to radiation damage among the three different crystals which have so far been studied in JUMBO. When the beryl crystals were initially installed no significant radiation damage was observed during several days exposure time. However, after several months of running time under dedicated conditions of ~50 mA and ~3 GeV at SSRL (corresponding to ~4000 watts hour cm^{-2} integrated radiation exposure), the rocking curves were again measured. The measured rocking curves were found to be ~25-30% larger than what had been found initially (Figs. 4 and 5). No significant physical damage to the crystals was observable except a faint radiation burning mark on the surface of the first beryl crystal. A dark burn mark was also observed on the Ge crystal after integrated radiation exposure of ~20,000 watts hour cm^{-2}, probably due to

cracking of hydrocarbons on the exposed surface. Insertion of the 1 mm slit can be used to cut down radiation damage.

VI. APPLICATIONS

In this Section several applications of JUMBO are given. For each example reference is made to the original publication(s) where the work in question is more fully described. In the brief summaries given below, our main emphasis is technical: the common theme is the capability of JUMBO in addressing a particular type of scientific problem.

VI.1 Angle-Resolved Photoemission Study of Bulk Valence Bands

Angle-resolved photoemission (ARP) spectroscopy is the technique of choice for studying the total valence-band structures of solids. We have carried out ARP experiments on the valence bands of W(011) using JUMBO in the energy region 1100-1250 eV to address two fundamental questions [18] pertaining to photoemission from metals:

(1) What is the dominant source of Brillouin-zone averaging in valence-band experiments at photon energies of ~1 keV: phonon-assisted nondirect transitions arising from lattice vibrations and/or complexities in the final-state electronic wave function due to scattering or component mixing by the crystal potential?

Either mechanism would suppress the importance of wave-vector conservation as a useful selection rule in determining which initial region in the Brilluoin zone is involved in the emission. The presence of phonon effects would imply a strong temperature dependence in ARP spectra. Inasmuch as phonon effects can be reduced at low temperatures and/or by selecting a system with the large Debye-Waller factor, one would expect to observe a strong excitation-energy dependence in ARP valence-band spectra if complexities in the final state electronic wave function are not important or vice versa.

(2) If direct transitions (DT) can be observed in ARP at higher energies under certain conditions, is it possible to analyze the data using a simple DT model previously shown to apply rather well to photoemission studies in the 40-150 eV range [19]?

Experimental valence-band spectra along normal-emission direction at excitation energies of 1100 eV, 1150 eV, 1175 eV, and 1200 eV, together with theoretically expected curves based on a simple DT model are shown in Fig. 16. There are marked changes in the relative intensities of the two prominent peaks at binding energies of ~2.3 eV and ~4.8 eV which are in very good agreement with the simple DT model.

It has also been observed, but not shown here, that these spectra exhibit very strong temperature dependences, such that at high temperatures they converge to nearly the same shape. This behavior is consistent with a strong DT component at lower temperatures and complete zone averaging due to phonon effects at higher temperatures.

We conclude that direct transitions can be observed in ARP valence-band spectra obtained at excitation energies of ~1 keV from materials with large Debye-Waller factors. Phonon-assisted non-direct transitions, rather than final-state complexity, are the dominant source of the Brillouin-zone averaging. A simple bulk direct-transition model with plane-wave final states and constant matrix elements gives a good description of spectral changes with photon energy. Furthermore, future ARP experiments with variable photon energies in the presently available region of ~800-1500 eV, combined with more favorable conditions of low temperatures ($\leq$100 K) and higher analyzer angular resolution ($\leq 2^{0}$) could provide a rather straightforward technique for studying the band structures of solids.

VI.2 Threshold Experiments in Photoelectron and Auger Spectroscopy

The high energy resolution of the crystal monochromator, in particular

of the beryl crystals, allows near-edge photoelectron and Auger studies of deep core levels. Spectra can be taken for photon excitation just below, at, and above the desired thresholds and even narrow (e.g. 1 eV wide) "white lines" can be investigated by studying the accompanying Auger decay. Therefore this monochromator opens a new energy range to study the transition from sudden to adiabatic limits in photoionization processes and to investigate relaxation, resonance effects, post-collision interaction (PCI) and details in the Auger fine structure such as double ionization satellites and Coster-Kronig transitions in solids, adsorbates, and gases.

An extensive study [20] of the threshold behavior of the famous ~6 eV satellite of Ni photoelectron peaks as well as of threshold effects in LMM Auger decays of both Ni and Cu, supports this conclusion. As an example, Figure 17 shows the $L_{2,3}VV$ ($V=M_{4,5}$) Auger spectra obtained from a Ni(001) single crystal at different photon energies around the Ni L-edges as indicated. The inset in Figure 17 displays the absorption edge fine structure of the Ni L_{III} and L_{II} edges recorded using partial electron yield. Note the steep onset at the L_{III} edge (about 1 eV wide), the high edge jump (a factor of 5) and the very intense L_{III} resonance (a factor of 15, relative to the pre-edge background).

In the spectra of Figure 17, L_3VV and L_2VV Auger transitions can be distinguished. The Ni-valence band structures are also shown moving from the L_3VV peaks to higher kinetic energies with increasing photon energies. The shape of the main structure around 848 eV (L_3VV) varies only slightly with increasing photon energy, while the L_2VV structure at 867 eV markedly changes its shape as well as its intensity relative to the main L_3VV transition indicating a varying rate of the competing $L_2 \rightarrow L_3V$ Coster-Kronig transition.

From our experimental results for Cu and Ni we can clearly show [20]: (1) There are no solid state PCI effects observable when approaching the thresholds. (2) There are only minor structural changes in the L_3VV features; in particular, ther is no marked difference between Cu and Ni, as in the case of electron excited spectra. (3) The low-kinetic-energy tail of the L_3VV main peak shows a steady intensity increase with photon energy, with some fine structure already being present at the L_{III} edge; this rules out double ionization satellites as a major contributor to this part of the spectrum; and (4) The intensity of the L_2VV transition is increasing rather than decreasing near the L_{II} threshold, in contrast to earlier results; marked structural changes near the L_{II} threshold have been observed.

It should be noted that most of the details of these spectra (e.g. the threshold behavior of the L_2VV transition) could only be studied because of the good energy resolution provided by JUMBO.

VI.3 Near Edge and EXAFS Studies of Sulfur in Various Coals

Sulfur is one of the major and most troublesome contaminants in fossil fuels. Although present only in low concentrations (typically 0.3 to 4% by weight), sulfur causes problems in every process that uses coal. Therefore any process for coal conversion or combustion must contain a strategy for dealing with the constituent sulfur. Unfortunately very little is known about the chemical structure of coal and the bonding properties of sulfur in particular. This is mainly true because of the absence of viable *in situ* investigations of sulfur in coal.

The installation of JUMBO has enabled a study of the near-edge x-ray absorption and the extended x-ray absorption fine structure (EXAFS) at the sulfur K-edge (2472 eV). A variety of standard coal samples and, for comparison, iron sulfide compounds of known stoichiometry have been investigated by detecting total electron yield as a function of photon energy [21].

As an example, Figure 18 shows selected near-edge spectra of four different coal samples. The first surprise in these spectra is that the "edge jump ratio" above background is so large (10 to 35%), in light of the low abundances of sulfur. The explanation lies in the fact that, except for iron and trace impurities, sulfur is by far the heaviest element present in coal. At 2472 eV the oscillator strengths of absorbing K-edges of carbon, nitrogen and oxygen are very low. Secondly, a large variation in the near-edge region can be observed; at least six peaks and shoulders of changing intensity are distinguishable. This is a nice example demonstrating that the analysis of near-edge structures is a promising technique for "fingerprinting" chemical structure on an in situ basis. Similar spectra from different iron sulfide compounds (FeS_x, x=1.09, 1.117, 2) support this approach [21]. The EXAFS spectra from iron sulfides and most coal samples possess good spectral contrast ratios, and enough oscillations are visible to encourage Fourier analysis in order to get reliable information about bond distances.

In conclusion, it appears that we have the basis of a useful spectroscopic method for in situ characterization of sulfur in fossil material, even in very low abundance.

VI.4 Electron Yield SEXAFS

JUMBO allows access to a variety of new absorption edges and offers significantly more flux and less scattered light than the grasshopper monochromator [15] which had previously been employed for SEXAFS measurements on low-Z adsorbates. Figure 19 shows the SEXAFS spectrum of the low-Z adsorbate sulfur on Ni(100) [22]. These data exhibit bulk-like signal-to-noise ratios and allow the precise determination of the chemisorption site as well as the S-Ni nearest neighbor distances on the surface.

Three SEXAFS spectra recorded at incidence angles $\theta = 10^{o}$, 45^{o} and 90^{o} yielded a S-Ni nearest neighbor distance within 0.01 Å. Including all sources of errors we conservatively quote the S-Ni distance on the surface to be 2.23 ± 0.02 Å which is 0.16 Å shorter than for bulk NiS. For $\theta = 90^{o}$ a second peak is observed in the Fourier transform of the SEXAFS signal. This peak, corresponding to a S-Ni second nearest neighbor distance of 4.15 ± 0.10 Å, unambiguously determines the fourfold hollow as the adsorption site.

The fourfold site is independently determined from comparison of experimental and calculated polarization dependent amplitude ratios. The experimentally determined ratio agrees to better than 4% with the theoretical value for the fourfold site and is more than a factor of 4 different from that for the twofold bridge or the atop sites. The accuracy of our relative amplitude determination was found to be better than ± 10% by comparing two pairs of data sets taken at 10^{o} and 90^{o}, and at 45^{o} and 90^{o}. This is comparable to the accuracy with which bulk data can be analyzed.

Finally the SEXAFS amplitudes were compared to that obtained for a bulk NiS standard for which each S atom is known to be surrounded by six Ni atoms. This procedure, as a third independent determination, again favors the fourfold hollow site. The absolute coordination numbers determined from experiment are all within 10% of the calculated values for the fourfold hollow site. This agreement is remarkable and again comparable with that obtained for bulk systems.

The present results demonstrate the state-of-the-art reliability and accuracy of SEXAFS on low-Z adsorbates on surfaces and of SEXAFS as a technique in general. In the past SEXAFS measurements often suffered from signal-to-noise problems which limited the inherent high accuracy of the technique for structure determinations. Experimental problems were most

severe for the technologically most important low-Z atoms where amplitude analysis has previously been unreliable or failed altogether [23]. The present results indicate that amplitude transferability problems previously encountered ror measurements on chemisorbed oxygen atoms must have been caused by scattered light problems which are often present for grating monochromators. The excellent monochromatic-to-scattered light ratios obtainable with crystal monochromators can thus provide high-reliability structure determinations by SEXAFS.

VI.5 Ion Yield SEXAFS

Photon-stimulated desorption (PSD) of ions from surfaces has recently been shown by Knotek, Jones and Rehn [24] to be coupled to the core-electron excitation process. Since all processes which are linked to filling a core hole created by photon absorption can provide a measure for the respective absorption coefficient, the PSD ion yield can be used as a signal for SEXAFS measurements.

Figure 20 shows the first PSD SEXAFS measurement [25]. It compares the total electron yield Mo L_I (2870 eV) EXAFS for a clean Mo(100) sample with the O^+ yield signal obtained from a Mo(100) surface exposed to 100 L oxygen. Owing to the high photon flux transmitted by JUMBO the O^+ signal strength was about 10^5 counts/sec. The oscillations above threshold are closely the same in frequency with an overall reduction in amplitude for the O^+ yield spectrum. The structures around 2840 eV and 3290 eV are caused by multiple Bragg reflection in the Mo(100) single crystal and in the Ge(111) monochromator crystals, respectively. Both structures can be removed as indicated by the dashed lines in Figure 20.

The electron yield EXAFS amplitude is larger by almost exactly a factor of 2($\pm$10%). Because the electron yield signal originates from atoms within

50-100 Å of the (100) surface the corresponding EXAFS spectrum is representative of bulk Mo atoms which are surrounded by 8 other Mo atoms. The O^+ yield SEXAFS signal originates from the Mo-Mo distance of a surface Mo atom with its 4 nearest Mo neighbors in the second layer, its amplitude is therefore reduced by a factor of 2. The Mo-O SEXAFS signal was not observed in the present study because the backscattering amplitude of the O atoms is smaller than that of the Mo surface atoms and because the low-k EXAFS region above the L_I edge contains a non-negligible contribution from the EXAFS above the L_{III} and L_{II} edges which lie 346 eV and 241 eV below the L_I edge, respectively.

The above measurements establish PSD as a new powerful detection technique for SEXAFS studies. PSD SEXAFS measurements can be carried out above both the substrate as well as the adsorbate absorption edges and offer thus additional information as compared to electron yield SEXAFS (adsorbate edge only) studies. JUMBO allows access to many substrate K and L absorption edges (all elements with Z < 50!) and thus enables PSD SEXAFS studies of the important low-Z atoms by exciting the higher-energy substrate edges.

VII. CONCLUSIONS AND FUTURE IMPROVEMENTS

We have discussed the performance of the first UHV compatible double-crystal monochromator JUMBO used to monochromatize synchrotron radiation in the spectral range 800-4500 eV. It is pointed out that the design of an instrument for the transition region between the VUV and hard x-ray regions warrents many new design features and several new problems have to be overcome. Specifically, it has been found that under the present conditions of the monochromator, the available independent motion of both crystals is absolutely necessary to keep crystals in phase as photon energy is scanned. This is obvious from the fact that the maximum correction required is as much as ~400 arc sec, which is a factor of 2-5 larger than

the typical FWHM of the crystal rocking curves. Furthermore, the temperature effects are so large that a feedback mechanism involving only piezo-electric crystals to tune the monochromator crystals for maximum flux is difficult and probably not adequate unless additional efforts are made to reduce temperature effects. A necessary step in further improving the performance of JUMBO definitely requires a temperature control system for the monochromator crystals. This could be partially accomplished either by cooling the top crystal and/or by using suitable filters, in addition to graphite filters which are being used presently, to further reduce thermal load and damage. More effectively, a major control on exposure of the top crystal to the unnecessary spectrum of the radiation can be achieved by utilizing a wide band pass monochromator carrying, for example, synthetic crystals such as boron-tungsten sandwiches as a first stage rough monochromator. Another possible approach may be the use of a variable incidence beam-splitter mirror which can filter out all x-ray radiation above a desired energy. These improvements will not only help to simplify the operation of the monochromator and to enhance resolution, but it will also enable the future use of crystals with large 2d spacings (e.g., the acid phthalates) which are very susceptible to radiation damage. After incorporating a suitable temperature control system in JUMBO, a feedback loop which is coupled to a piezo-electric rocking motion of one of the crystals appears to have advantages over the present scheme. Such a system would have a faster and more flexible response than a feedback loop stopping one of the goniometers, and would also fascilitate finding the maximum more precisely (probably within 1-2 arc sec).

ACKNOWLEDGEMENTS

The implementation of JUMBO required help from many people at various stages of the project. We would like to acknowledge Seth Goldberg and

R. Z. Bachrach for implementing the computer software, Richard Boyce for solving some of the mechanical stability problems, Fuat Deniz Dikmen for carrying out calculations on thermal effects and we would like to thank John Barton, Rolf Jaeger, Sean Brennan, and J. Haase for their help in debugging JUMBO and taking some of the presented data. One of us (Z. H.) would like to thank Nathan Spielberg, Burton Henke, and Richard D. Deslattes for very useful discussions and Winifred Hepler for preparation of the monochromator crystals. One of us (E. U.) acknowledges a research grant from the Deutsche Forschungsgemeinschaft. This work was supported by the Director, Office of Energy Research, Office of Basic Energy Sciences, Chemical Sciences Division of the U.S. Department of Energy under Contract No. W-7405-ENG-48. It was performed at the Stanford Synchrotron Radiation Laboratory, which is supported by the NSF Grant No. DMR 77-27489, in cooperation with the Stanford Linear Accelerator Center.

References:

1. H. Winick and S. Doniach, editors, Synchrotron Radiation Research (Plenum Press, New York, 1980).
2. K. Codling, Nucl. Instr. and Meth. 172 (1980) 107-122.
3. M. R. Howells, Nucl. Instr. and Meth. 172 (1980) 123-131.
4. R. D. Deslattes, Nucl. Instr. and Meth. 172 (1980) 201-208.
5. J. Cerino, J. Stöhr, N. Hower and R. Z. Bachrach, Nucl. Instr. and Meth. 172 (1980) 227-236.
6. A double-crystal monochromator which is not UHV compatible and does not have any focusing mirror is described by M. Lemonnier, O. Collet, C. Depantex, J. M. Estena and D. Raoux, Nucl. Inst. and Meth. 152 (1978) 109.
7. J. A. Howell and P. Horowitz, Nucl. Instr. and Meth. 125 (1975) 225.
8. J. Hastings, B. M. Kincaid and P. Eisenberger, Nucl. Instr. and Meth. 152 (1978) 167.
9. N. Spielberg, Ph.D. Dissertation, The Ohio State University, Columbus, Ohio, 1952; J. Korringer, E. J. Jossem, R. Liefeld, R. E. Kvardon and C. H. Shaw, Technical Report No. 7, Department of Physics and Astronomy, The Ohio State University, Columbus, Ohio, 1957.
10. Y. Gosh, O. Hirao, M. Murata, T. Tanoue and M. Tsuruoka, X-ray Spectr. 4 (1975) 74.
11. G. Brogen, Ark. Fys. 22 (1962) 267.
12. D. M. Barrus, R. L. Blake and A. J. Burek, X-ray Spectr. 5 (1976) 92; A. J. Burek in X-ray Instr. Workshop Edit. H. Winick and G. Brown, SSRL Report No. 78/04.
13. N. G. Alexandropoulos and G. G. Cohen, App. Spectr. 28 (1974) 155.
14. L. I. Johansson and J. Stöhr, unpublished results.

15. F. C. Brown, R. Z. Bachrach and N. Lien, Nucl. Instr. and Meth. 152 (1978) 73.

16. H. P. King and L. E. Alexander, X-ray Diffraction Procedures (Wiley, N.Y., 1974).

17. J. Stöhr, R. Jaeger, J. Feldhaus, S. Brennan, D. Norman and G. Apai, Appl. Optics 19, 3911 (1980).

18. Z. Hussain, E. Umbach, J. J. Barton, J. G. Tobin, and D. A. Shirley Phys. Rev. B (to be published).

19. Z. Hussain, S. Kono, L. G. Petersson, C. S. Fadley, and L. F. Wagner, Phys. Rev. B 23, 724 (1981) and references therein.

20. E. Umbach, Z. Hussain, J. J. Barton, C. C. Parks, J. G. Tobin, and D. A. Shirley, SSRL Report No. 81/02.

21. Z. Hussain, J. J. Barton, E. Umbach, and D. A. Shirley, SSRL Report No. 81/02.

22. S. Brennan, J. Stöhr, and R. Jaeger Phys. Rev. B (to be published).

23. J. Stöhr, L. I. Johansson, I. Lindau, and P. Pianetta, Phys. Rev. B20, 664 (19~9). J. Stöhr, L. I. Johansson, S. Brennan, M. Hecht, and J. N. Miller, Phys. Rev. B22, 4052 (1980).

24. M. L. Knotek, V. O. Jones, and V. Rehn, Phys. Rev. Lett. 43, 300 (1979).

25. R. Jaeger, J. Feldhaus, J. Haase, J. Stöhr, Z. Hussain, D. Menzel, and D. Norman, Phys. Rev. Lett. 45, 1870 (1980).

Figure Captions:

Fig. 1 (a) Schematic of the monochromator elements and their positions from the source. (b) Depiction of the scanning of the monochromator to achieve a constant deviation device.

Fig.2 Schematic of the maximum search feedback mechanism.

Fig.3 The energy ranges of different monochromator crystals are compared. Energy regions marked with (i) solid lines have already been tested, (ii) dash-dotted lines will be covered in the future, and (iii) dashed lines may be used but with restrictions. The accessible K-absorption edges are indicated.

Fig. 4 Double crystal rocking curves of beryl($10\bar{1}0$) in the nondispersive mode (1,-1).

Fig. 5 The FWHM of (1,-1) rocking curves as a function of photon energy for beryl ($10\bar{1}0$), InSb(111) and Ge(111).

Fig. 6 The transmission function of JUMBO obtained using the beryl($10\bar{1}0$) monochromator crystals. Structures above 1550 eV are due to absorption near the K-edges of A and Si which are constituents of beryl.

Fig. 7 The transmission function using InSb(111) monochromator crystals. Absorption structures are present at the Pt M-edges and at the L-edges, as well as a few crystal glitches which arose from multiple Bragg reflections in the crystals.

Fig. 8 The transmission function in the energy range 2000-4500 eV using the Ge(111) monochromator crystals. In addition to Pt M-edges due to absorption by the Pt-coated mirror, a few crystal glitches are also present.

Fig. 9 Total electron yield curve of crystalline NaCl showing EXAFS above the Na K-edge. Data were obtained using beryl monochromator crystals.

Fig. 10 Total electron yield curve near Si K-edge from Si(111) with (7x7)LEED overstructure. Data were obtained using the InSb monochromator crystal.

Fig. 11 Total electror yield spectra from NiS showing near edge and EXAF structures above the S K-edge using the Ge monochromator crystals.

Fig. 12 Total yield EXAFS spectra from a fused quartz (SiO_2) sample using the InSb crystals. These spectra demonstrate how well the structures present in the transmission function could be normalized out.

Fig. 13 Difference curves showing corrections required for the top crystal to bring it in phase with the lower crystal for (a) wide entrance slit (3mm) and (b) narrow slit (1mm). Experimental curves are shown as solid lines and the calculated curves as dashed lines.

Fig. 14 Calculated difference between intended and actual photon energies plotted versus intended energies for various temperature differences of the two monochromator crystals.

Fig. 15 Sulfur is photoemission spectra obtained with two different entrance slit sizes. The observed peak shift and the increase in FWHM are caused by a change in temperature difference of the monochromator crystals.

Fig. 16 Valence-band photoemission spectra obtained for normal electron emission at four different excitation energies, compared with the direct-transition theory.

Fig. 17 L_3VV ($V=M_{4,5}$) and L_2VV Auger spectra from a Ni single crystal obtained at different photon energies around the L_{III} and L_{II}

absorption edges. The inset shows the absorption edge fine structures in a partial electron yield mode using secondary electrons.

Fig. 18 Near-edge structures of the sulfur K-edge in four different coal samples. Independently determined sulfur percentages (by weight) are also given.

Fig. 19 Sulfur K-edge SEXAFS spectrum for c(2x2) (half monolayer) S on Ni(100) recorded at 45^{0} x-ray incidence. The SEXAFS oscillations after background subtraction are shown in the lower half.

Fig. 20 Comparison of the total electron yield EXAFS for a clean Mo(100) sample (a) and the PSD O^{+} yield for 100 L O_2 on Mo(100) (-oxygen phase) (b) above the Mo L_1 edge. The structures at 2840 eV and 3290 eV are Bragg glitches as discussed in the text.

(a) CRYSTAL MONOCHROMATOR
BRANCH LINE

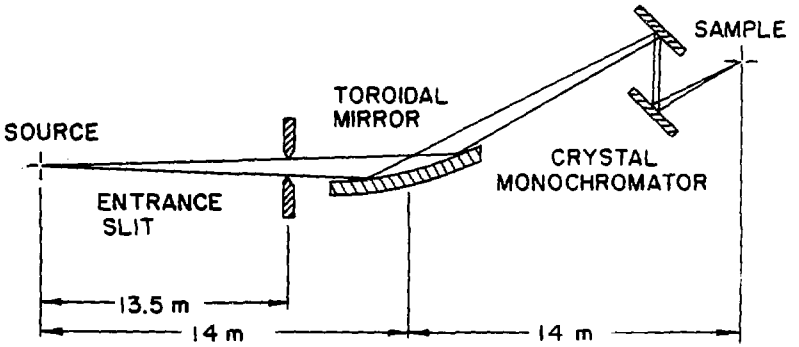

(b) CRYSTAL MONOCHROMATOR
(SIDE VIEW)

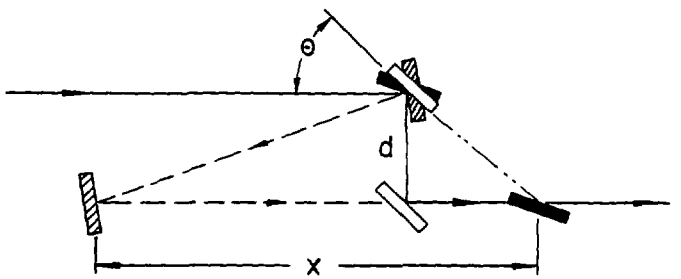

XBL 817-10639

Figure 1

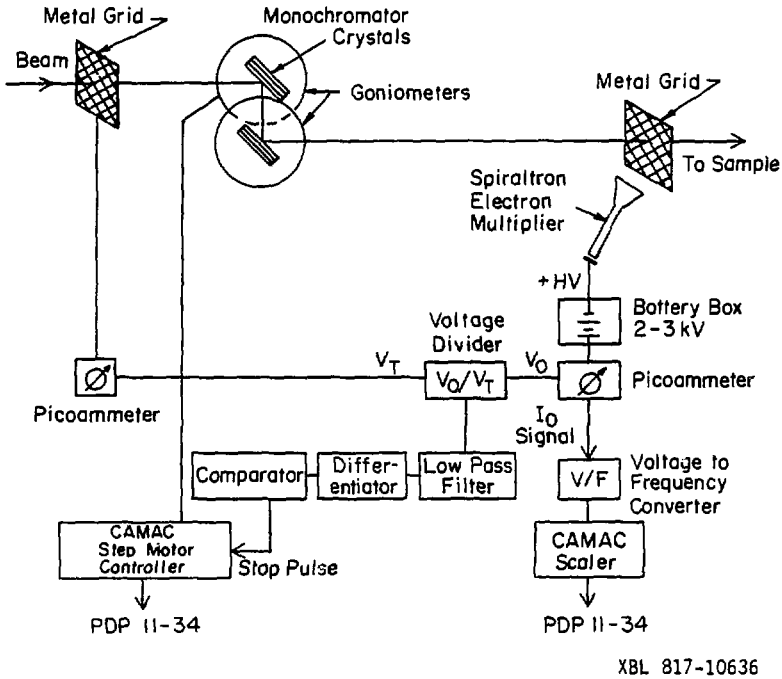
Metal Grid
Monochromator Crystals
Beam
Goniometers
Metal Grid
To Sample
Spiraltron Electron Multiplier
+HV
Battery Box 2-3 kV
Voltage Divider
V_T
V_O/V_T
V_O
Picoammeter
Picoammeter
I_O Signal
Comparator
Differ-entiator
Low Pass Filter
V/F
Voltage to Frequency Converter
CAMAC Step Motor Controller
Stop Pulse
CAMAC Scaler
PDP 11-34
PDP 11-34
XBL 817-10636

Figure 2

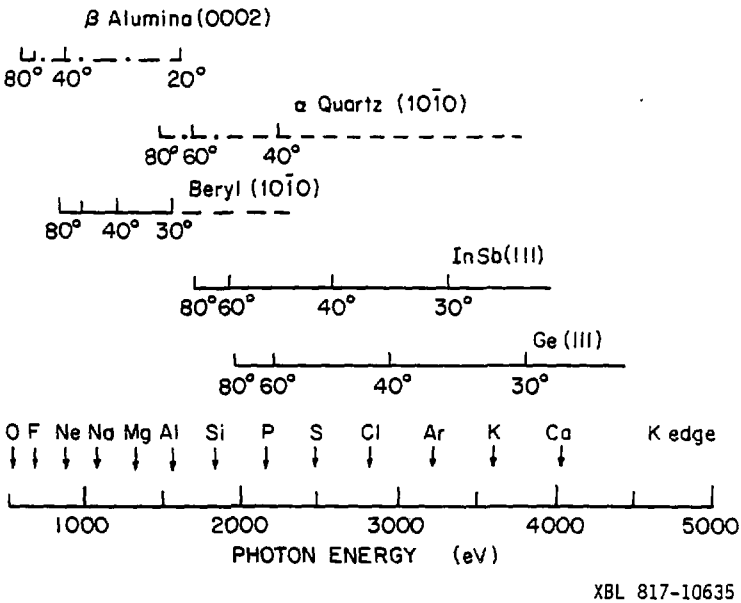
β Alumina (0002)
80° 40° 20°
α Quartz (10$\bar{1}$0)
80° 60° 40°
Beryl (10$\bar{1}$0)
80° 40° 30°
InSb(111)
80° 60° 40° 30°
Ge (111)
80° 60° 40° 30°
O F Ne Na Mg Al Si P S Cl Ar K Ca K edge
1000 2000 3000 4000 5000
PHOTON ENERGY (eV)
XBL 817-10635

Figure 3

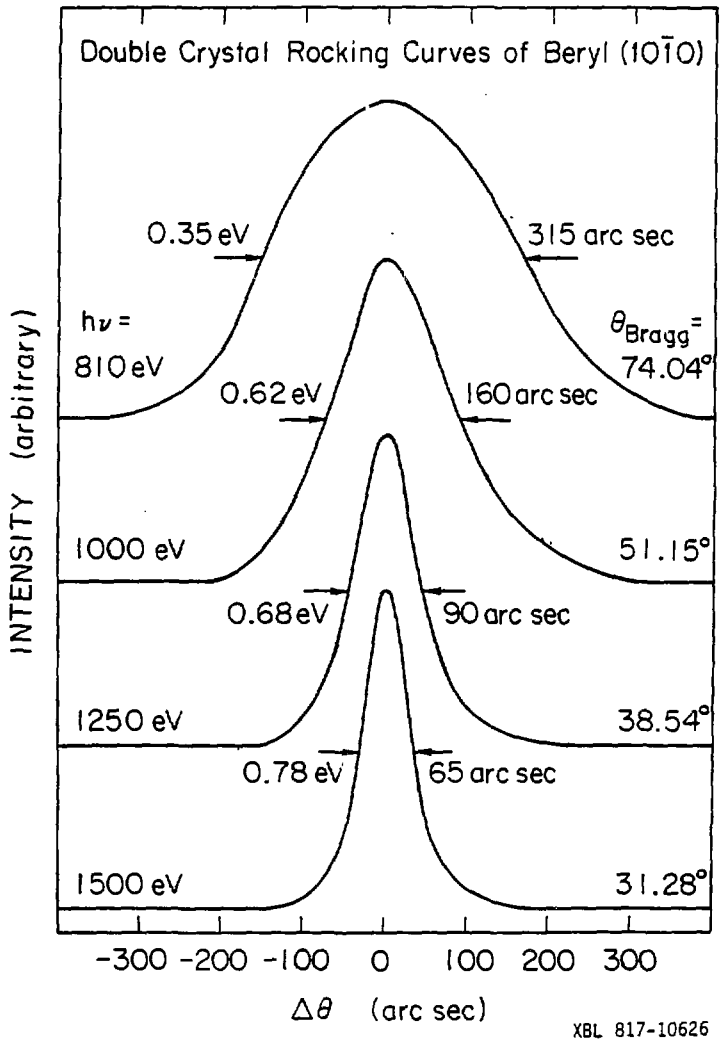
Double Crystal Rocking Curves of Beryl (10$\bar{1}$0)
INTENSITY (arbitrary)
0.35 eV
315 arc sec
hν = 810 eV
θ_{Bragg} = 74.04°
0.62 eV
160 arc sec
1000 eV
51.15°
0.68 eV
90 arc sec
1250 eV
38.54°
0.78 eV
65 arc sec
1500 eV
31.28°
-300 -200 -100 0 100 200 300
Δθ (arc sec)
XBL 817-10626

Figure 4

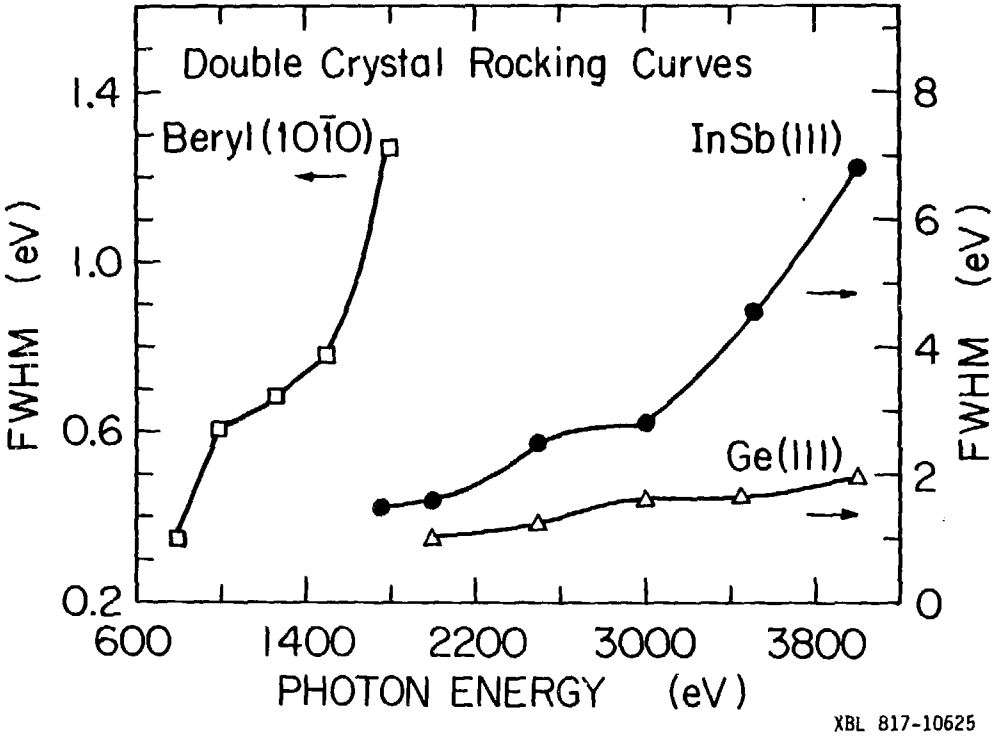
Double Crystal Rocking Curves
Beryl(10$\bar{1}$0)
InSb(111)
Ge(111)
FWHM (eV)
FWHM (eV)
1.4
1.0
0.6
0.2
8
6
4
2
0
600
1400
2200
3000
3800
PHOTON ENERGY (eV)
XBL 817-10625

Figure 5

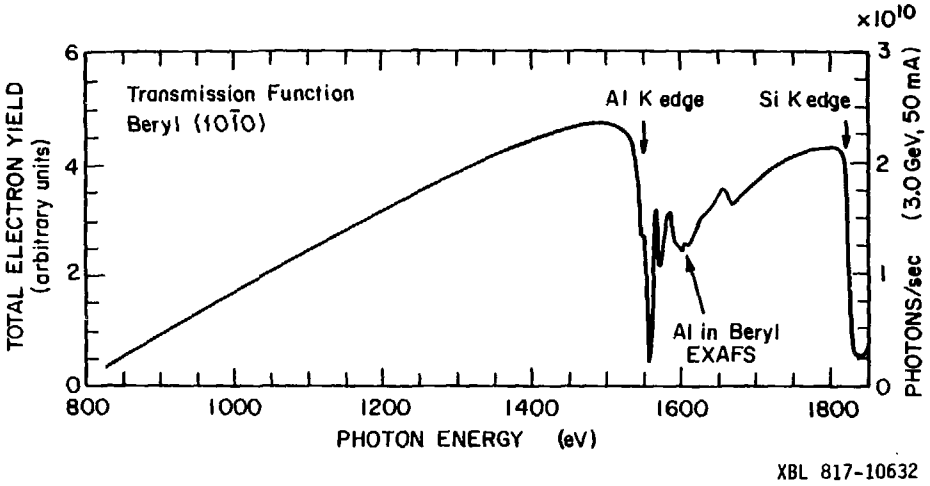

XBL 817-10632

Figure 6

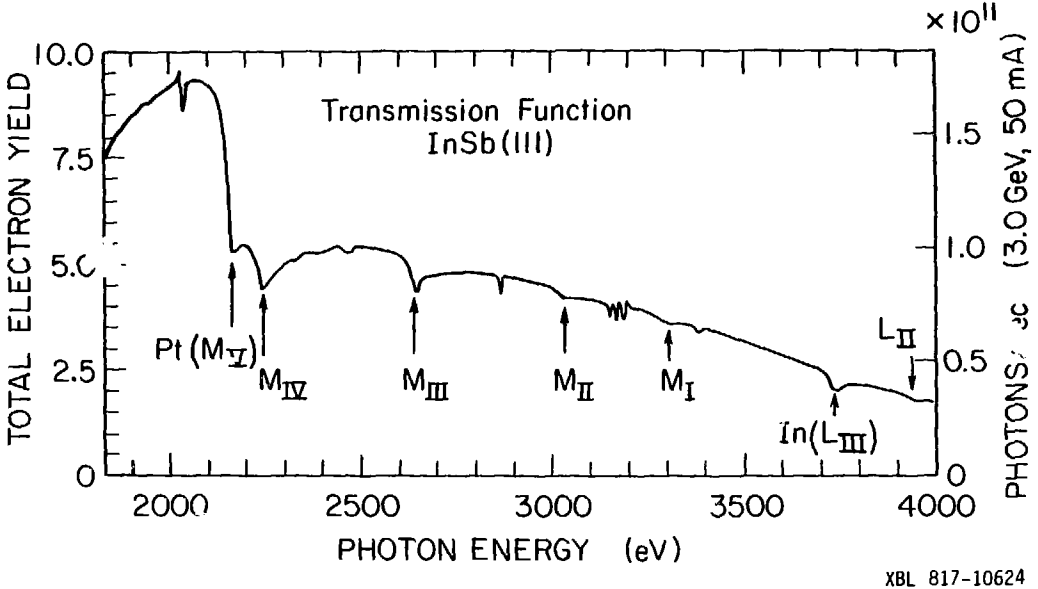
Transmission Function
InSb(III)
TOTAL ELECTRON YIELD
PHOTONS/ μc (3.0 GeV, 50 mA)
×10¹¹
10.0
7.5
5.0
2.5
0
1.5
1.0
0.5
0
Pt (M_V)
M_IV
M_III
M_II
M_I
L_II
In(L_III)
2000
2500
3000
3500
4000
PHOTON ENERGY (eV)
XBL 817-10624

Figure 7

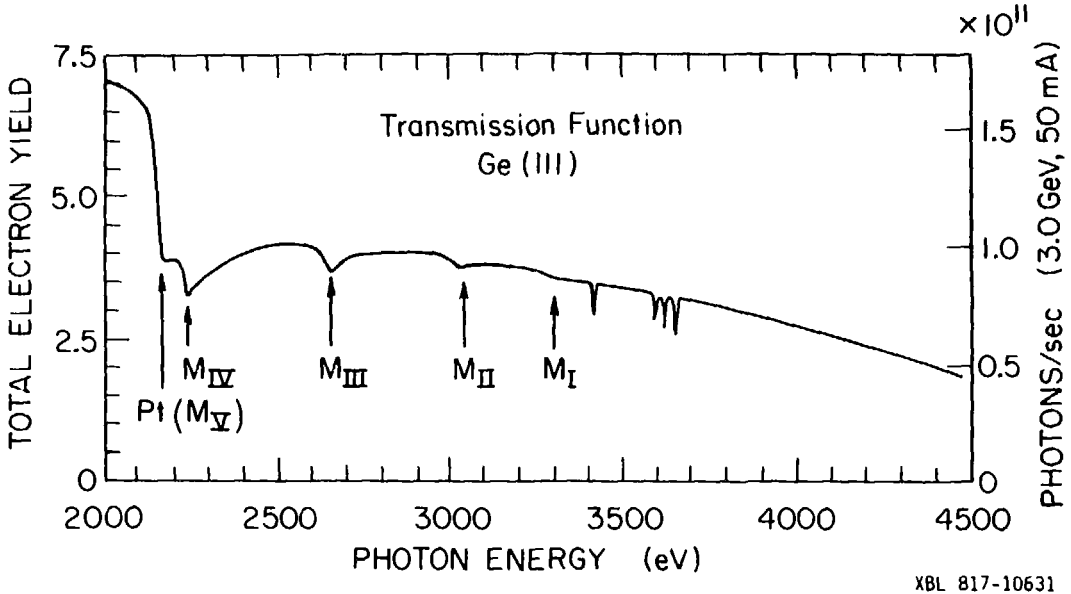
×10^11
7.5
5.0
2.5
0
TOTAL ELECTRON YIELD
Transmission Function
Ge (III)
1.5
1.0
0.5
0
PHOTONS/sec (3.0 GeV, 50 mA)
M_IV
M_III
M_II
M_I
Pt (M_V)
2000
2500
3000
3500
4000
4500
PHOTON ENERGY (eV)
XBL 817-10631

Figure 8

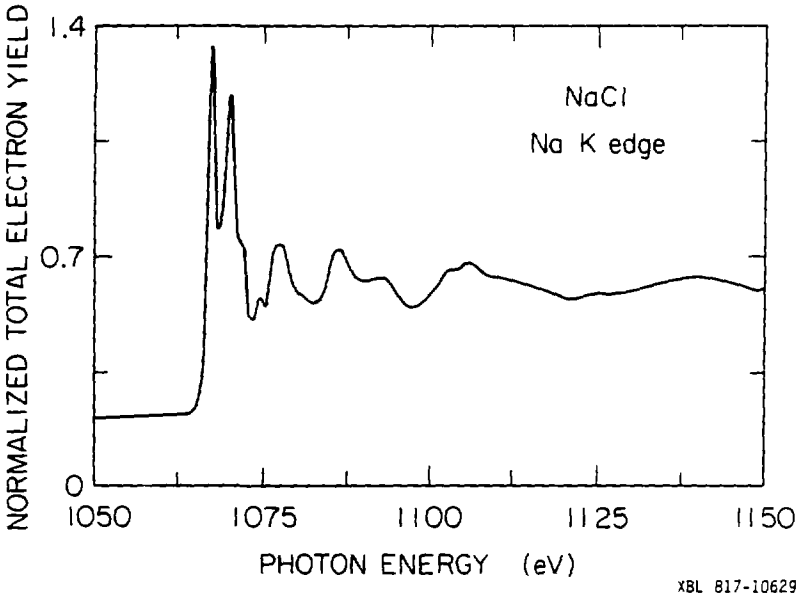
NORMALIZED TOTAL ELECTRON YIELD
1.4
0.7
0
NaCl
Na K edge
1050
1075
1100
1125
1150
PHOTON ENERGY (eV)
XBL 817-10629

Figure 9

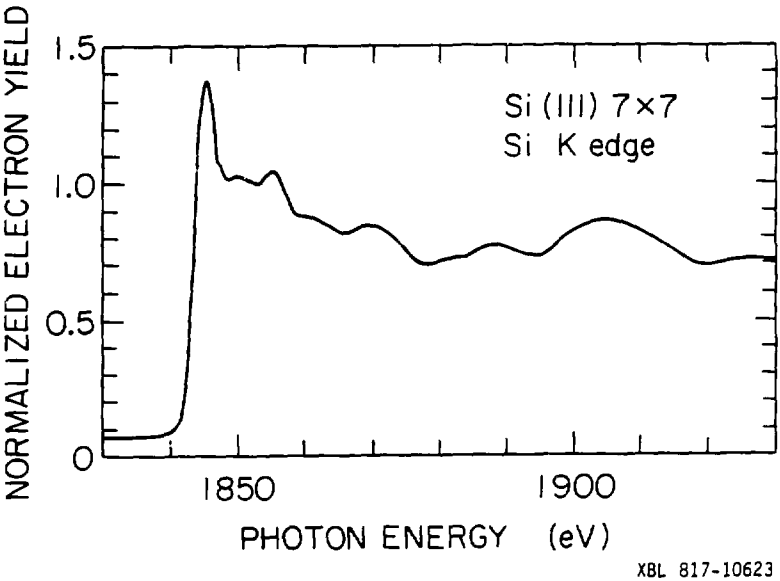
NORMALIZED ELECTRON YIELD
1.5
1.0
0.5
0
Si (III) 7×7
Si K edge
1850
1900
PHOTON ENERGY (eV)
XBL 817-10623

Figure 10

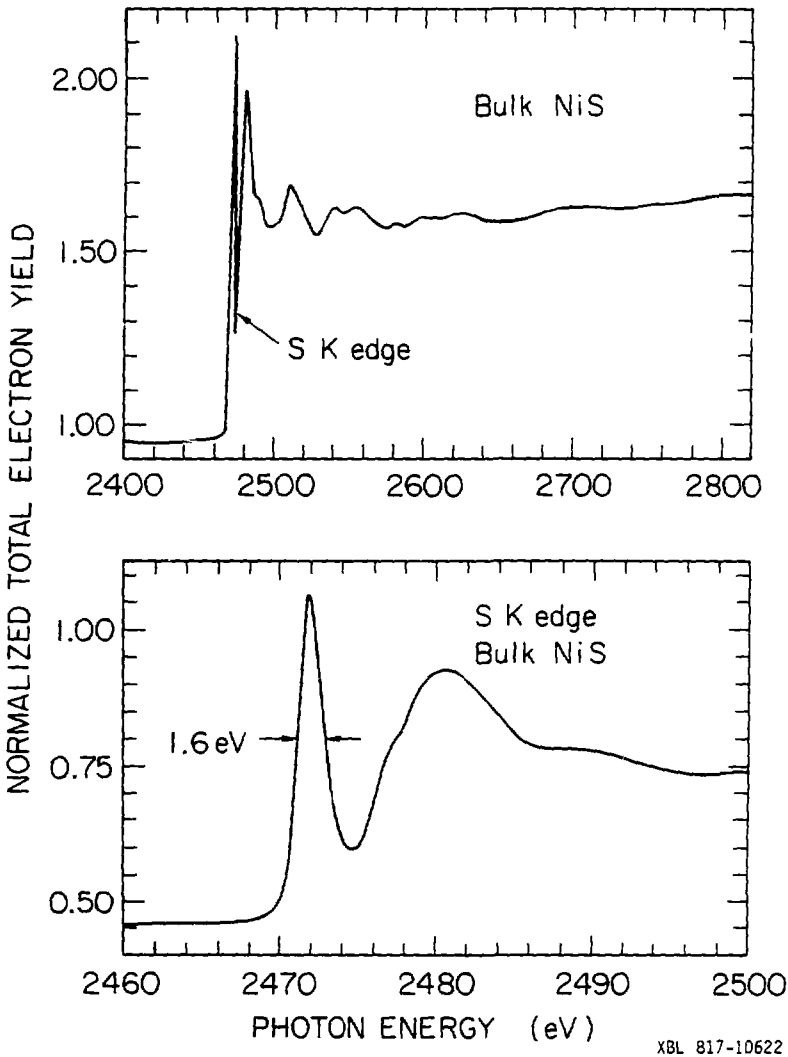
Bulk NiS
S K edge
2.00
1.50
1.00
2400
2500
2600
2700
2800
S K edge
Bulk NiS
1.6 eV
1.00
0.75
0.50
2460
2470
2480
2490
2500
NORMALIZED TOTAL ELECTRON YIELD
PHOTON ENERGY (eV)
XBL 817-10622

Figure 11

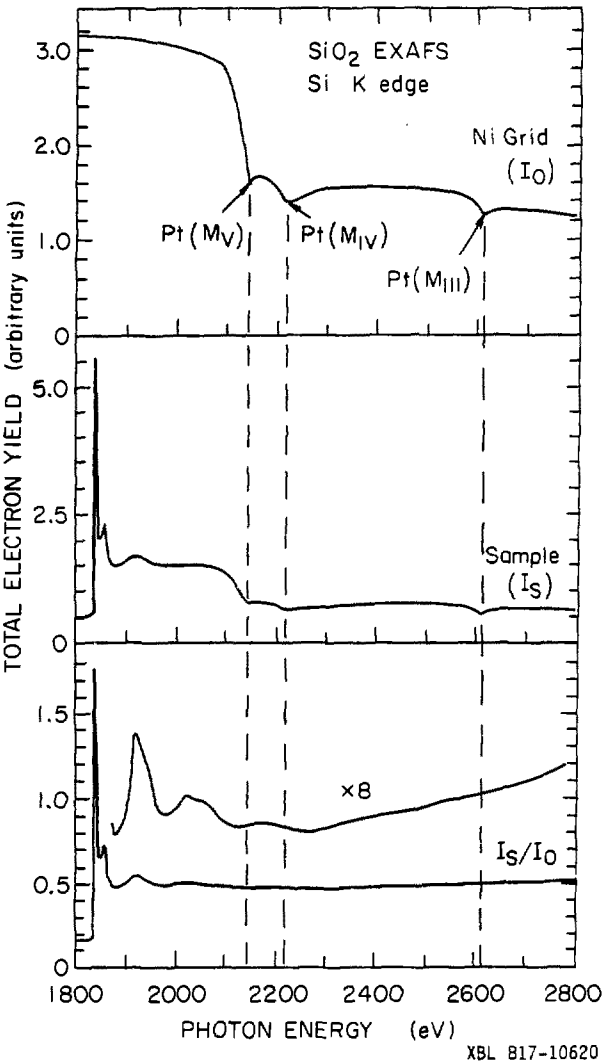
SiO2 EXAFS
Si K edge
Ni Grid
(I0)
Pt(MV)
Pt(MIV)
Pt(MIII)
Sample
(IS)
×8
IS/I0
TOTAL ELECTRON YIELD (arbitrary units)
PHOTON ENERGY (eV)
XBL 817-10620

Figure 12

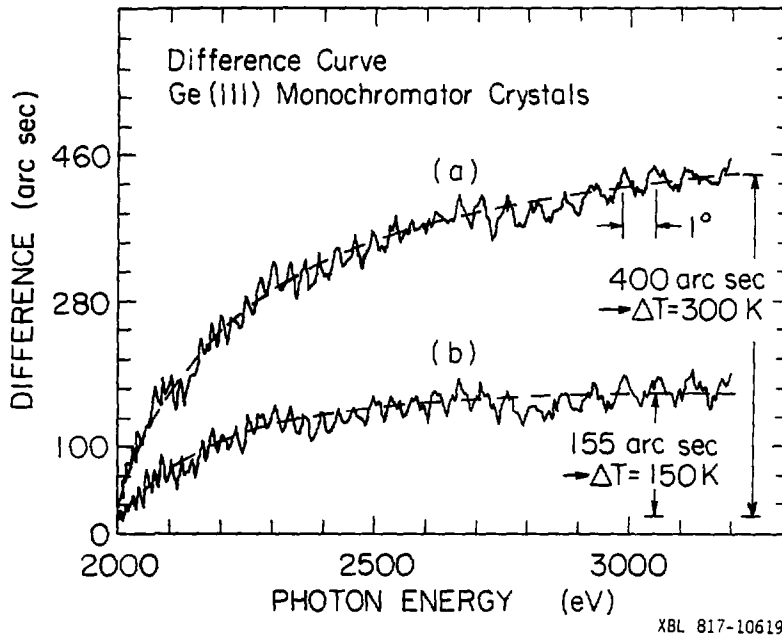
Difference Curve
Ge (111) Monochromator Crystals
DIFFERENCE (arc sec)
460
280
100
0
(a)
1°
400 arc sec
→ΔT=300 K
(b)
155 arc sec
→ΔT= 150K
2000
2500
3000
PHOTON ENERGY (eV)
XBL 817-10619

Figure 13

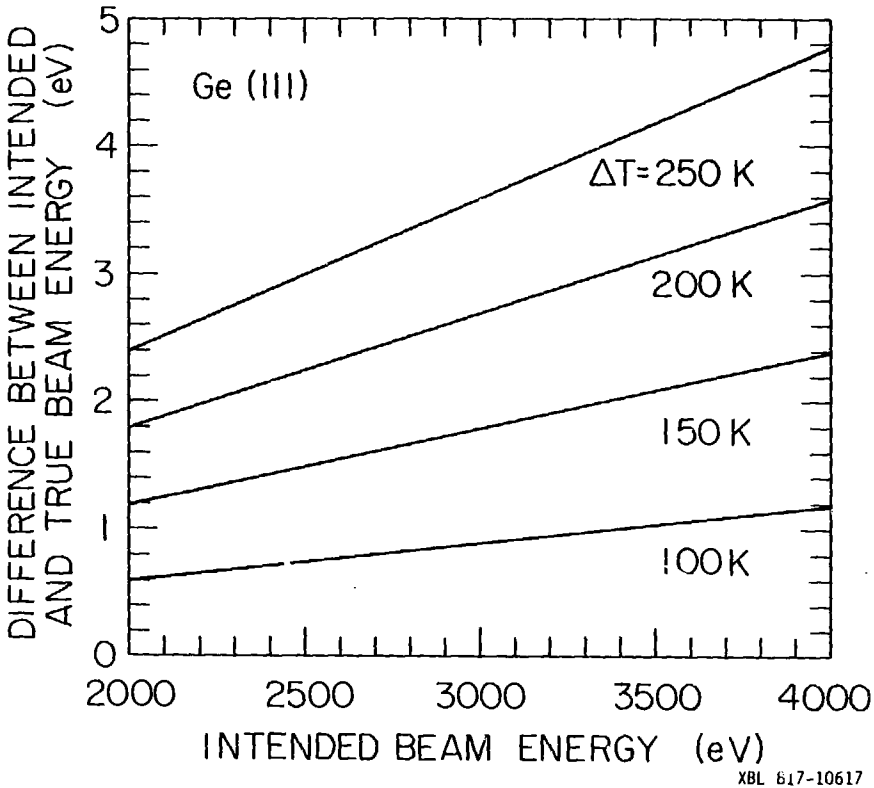
Ge (111)
ΔT=250 K
200 K
150 K
100 K
DIFFERENCE BETWEEN INTENDED AND TRUE BEAM ENERGY (eV)
INTENDED BEAM ENERGY (eV)
0
1
2
3
4
5
2000
2500
3000
3500
4000
XBL 817-10617

Figure 14

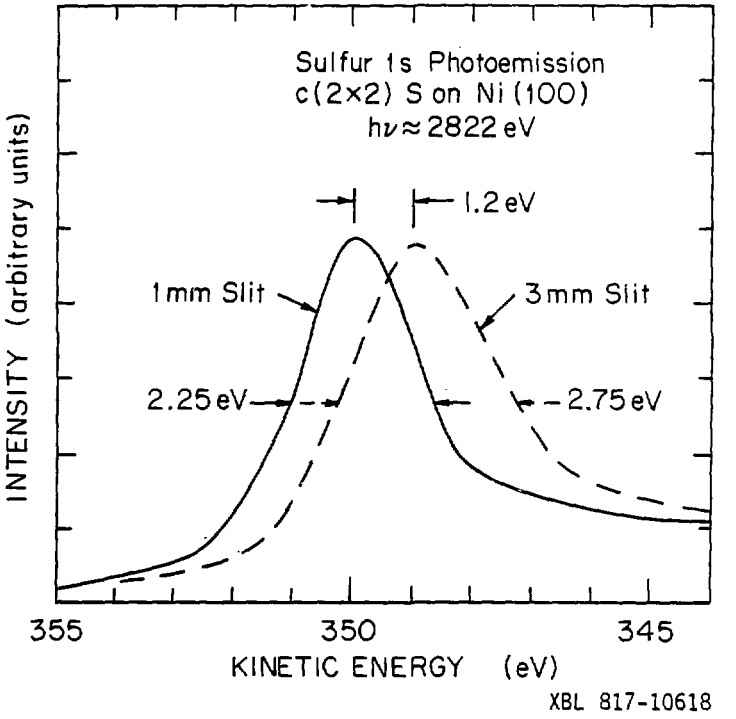
Sulfur 1s Photoemission
c(2×2) S on Ni (100)
hν≈2822 eV
1.2 eV
1mm Slit
3mm Slit
2.25 eV
2.75 eV
INTENSITY (arbitrary units)
355
350
345
KINETIC ENERGY (eV)
XBL 817-10618

Figure 15

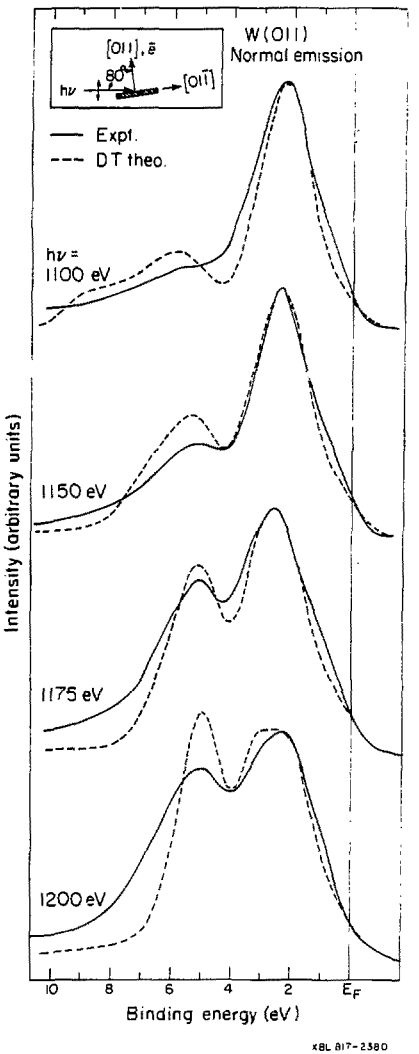
W(011)
Normal emission
[011], ē
80°
hν
[01$\bar{1}$]
Expt.
DT theo.
hν =
1100 eV
1150 eV
1175 eV
1200 eV
Intensity (arbitrary units)
10
8
6
4
2
E_F
Binding energy (eV)
XBL 817-2380

Figure 16

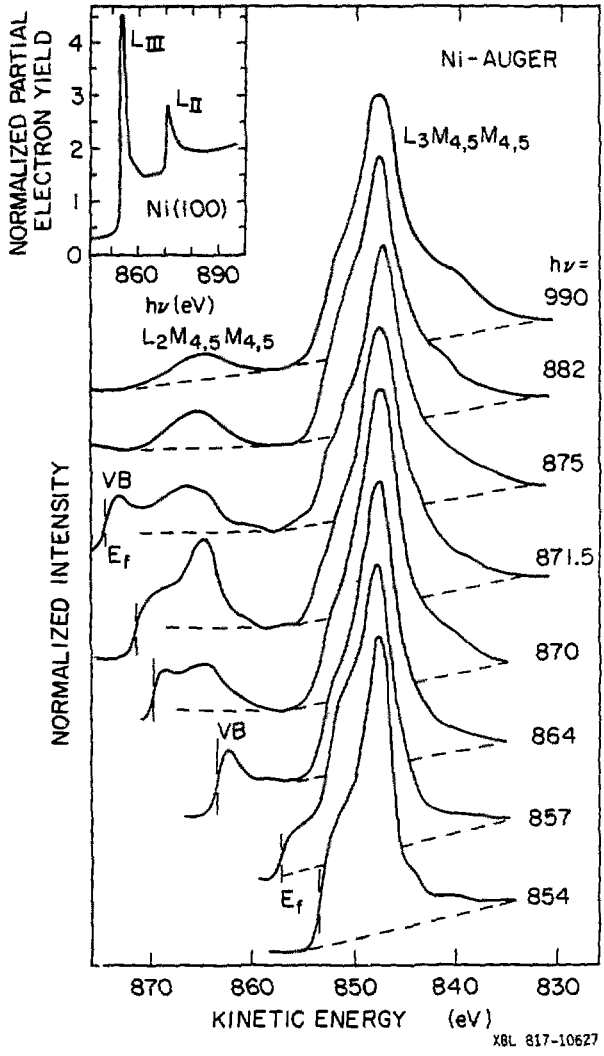
NORMALIZED PARTIAL ELECTRON YIELD
L_III
L_II
Ni(100)
hν(eV)
Ni-AUGER
L3M4,5M4,5
hν=
990
882
875
871.5
870
864
857
854
L2M4,5M4,5
VB
Ef
NORMALIZED INTENSITY
KINETIC ENERGY (eV)
XBL 817-10627

Figure 17

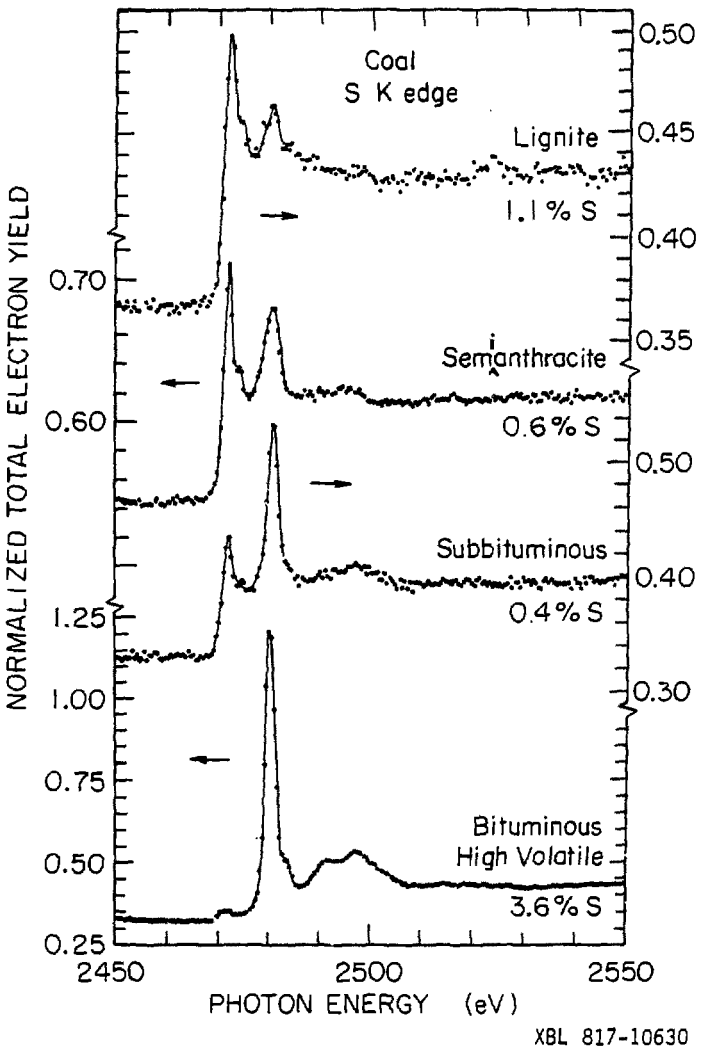
Coal
S K edge
Lignite
1.1 % S
Semianthracite
0.6 % S
Subbituminous
0.4 % S
Bituminous
High Volatile
3.6 % S
NORMALIZED TOTAL ELECTRON YIELD
0.70
0.60
1.25
1.00
0.75
0.50
0.25
0.50
0.45
0.40
0.35
0.50
0.40
0.30
2450
2500
2550
PHOTON ENERGY (eV)
XBL 817-10630

Figure 18

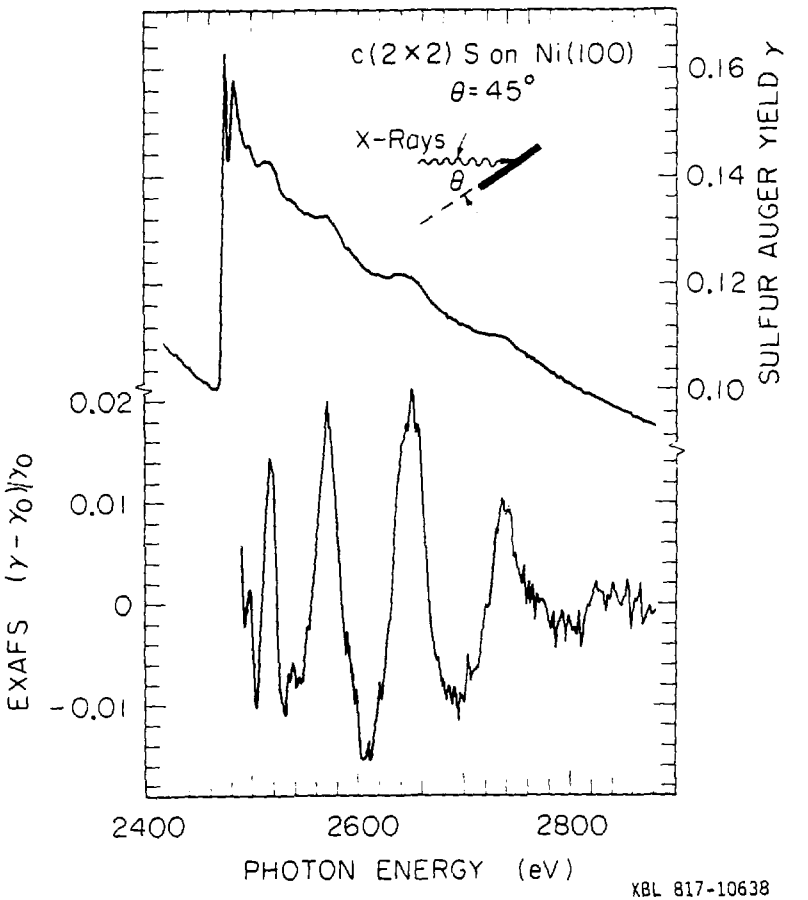
c(2×2) S on Ni(100)
θ = 45°
X-Rays
θ
0.16
0.14
0.12
0.10
SULFUR AUGER YIELD Y
0.02
0.01
0
-0.01
EXAFS (γ - γ0)/γ0
2400
2600
2800
PHOTON ENERGY (eV)
XBL 817-10638

Figure 19

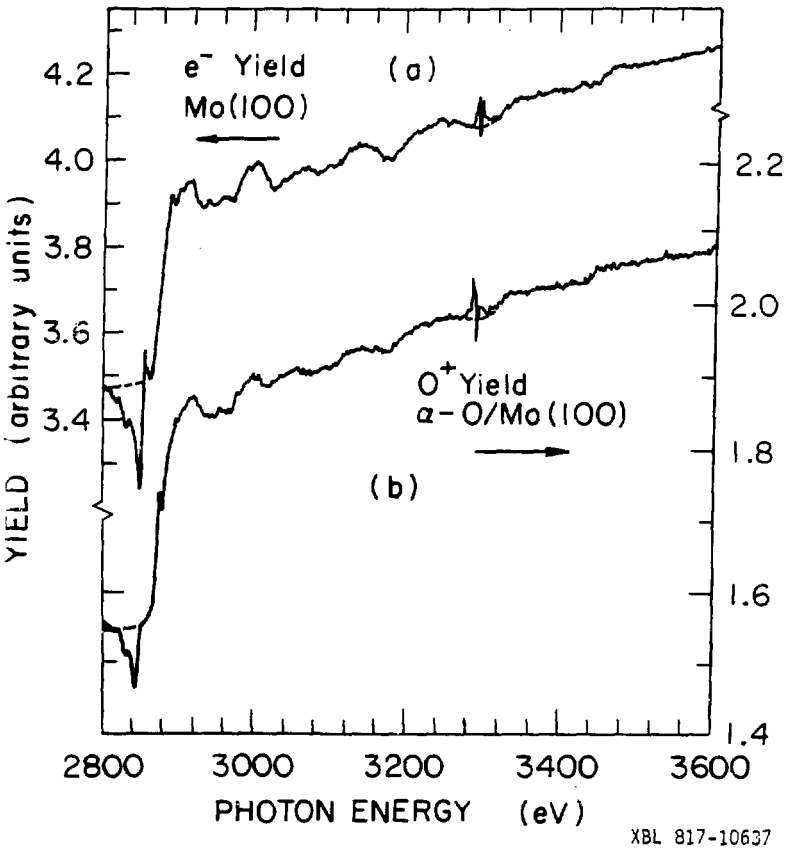
e⁻ Yield
Mo(100)
(a)
O⁺ Yield
α-O/Mo(100)
(b)
YIELD (arbitrary units)
4.2
4.0
3.8
3.6
3.4
2.2
2.0
1.8
1.6
1.4
2800
3000
3200
3400
3600
PHOTON ENERGY (eV)
XBL 817-10637

Figure 20